

Efficient electrical spin readout of NV⁻ centers in diamond

Florian M. Hrubesch,^{*} Georg Braunbeck, Martin Stutzmann, Friedemann Reinhard,[†] and Martin S. Brandt[‡]
*Walter Schottky Institut and Physik-Department,
 Technische Universität München, Am Coulombwall 4, 85748 Garching, Germany*

Using pulsed photoionization the coherent spin manipulation and echo formation of ensembles of NV⁻ centers in diamond are detected electrically realizing contrasts of up to 17%. The underlying spin-dependent ionization dynamics are investigated experimentally and compared to Monte-Carlo simulations. This allows the identification of the conditions optimizing contrast and sensitivity which compare favorably with respect to optical detection.

The nitrogen vacancy center NV⁻ in diamond is a promising candidate for quantum applications, since its coherence time at room temperature is in the range of ms [1] and its spin can be read out by optical fluorescence detection [2]. These features have enabled the use of NV⁻ centers, e.g., as a quantum sensor for magnetic fields [3, 4] and temperature [5], for scanning-probe spin imaging [6] and structure determination of single biological molecules [7]. Despite its apparent simplicity, however, optical spin readout has drawbacks: it is highly inefficient, requiring several 100 repetitions for a single spin readout, and cumbersome to implement in many applications. Electric readout of spin in a suitable diamond semiconductor device appears as an attractive way to surmount these limitations. It could enable access to NV⁻ centers in dense arrays, with a spacing limited by the few-nm-small feature size of electron beam lithography [8] rather than the optical wavelength. It might, moreover, provide a way to read out other spin defects [9–11], potentially including optically inactive ones.

Two methods for electric readout of NV⁻ centers have been demonstrated. The method in Ref. 12 uses non-radiative energy transfer to graphene and detects the spin signal in the current through the graphene sheet generated by this transfer. In contrast, the method presented in Ref. 13 uses the charge carriers generated directly in the diamond host crystal by photoionization of the NV⁻ centers (photocurrent detection of magnetic resonance, PDMR). Both methods, however, have until now only been used with continuous wave (cw) spin manipulation and have therefore remained limited to NV⁻ detection. Here we demonstrate a scheme based on both pulsed spin manipulation and pulsed photoionization to truly read out the spin state of NV⁻ centers electrically after coherent control, using Rabi oscillations and echo experiments as examples. We employ this scheme to establish a quantitative model of photoionization, simulate the readout efficiency and predict, that under optimized conditions pulsed electric readout could outperform optical fluorescence detection.

The spin-dependent photoionization cycle can be understood as an effective four-photon process, whose spin dependence relies on the NV⁻ center's inter-system crossing (ISC) which is also key to the classic optical readout

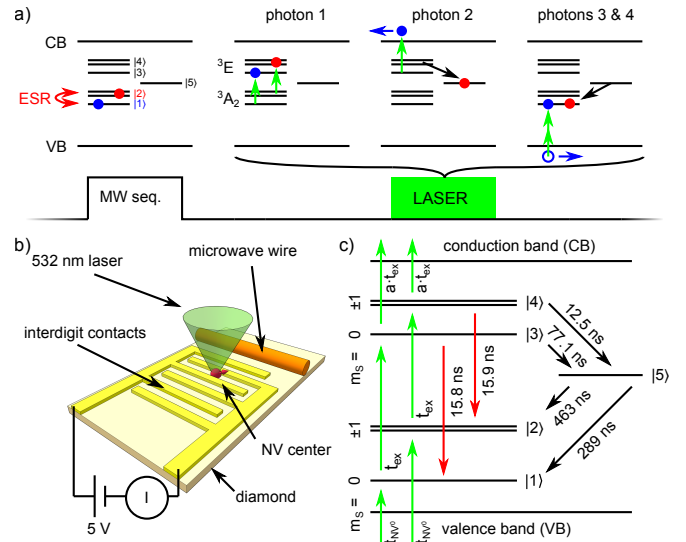


Figure 1. a) Spin-dependent photoionization of NV⁻ centers used for the electrical readout of its spin state. b) Schematic drawing of the sample and the measurement setup. c) Level scheme used for the Monte-Carlo simulation.

(Fig. 1 a)) [13]. A first photon (green arrows) triggers shelving (black arrow) of NV⁻ centers in spin state |2> (corresponding to the $m_S = \pm 1$ spin quantum numbers of NV⁻) into the long-lived metastable singlet state |5> by this ISC. Since shelving protects this spin state from further laser excitation, absorption of a second photon preferentially ionizes NV⁻ centers prepared in spin state |1> (corresponding to $m_S = 0$) into the conduction band (CB), creating a spin-dependent photocurrent (blue arrow) proportional to the population of the $m_S = 0$ state obtained by a microwave pulse sequence (red arrow) preceding the optical pulse. Two further photons re-charge the NV⁰ center into its negative charge state by exciting the NV⁰ (photon 3) and capture of an electron (photon 4) from the valence band (VB) [14].

Our spin readout experiments are performed in a photoconductor as shown in Fig. 1 b). We illuminate a densely NV⁻-doped diamond (Element 6, grown by chemical vapor deposition, with $[N] < 1$ ppm, $[NV] \approx 10$ ppb) with a green laser (wavelength 532 nm) pulse generated by a Nd:YAG laser and an acousto-optic modulator

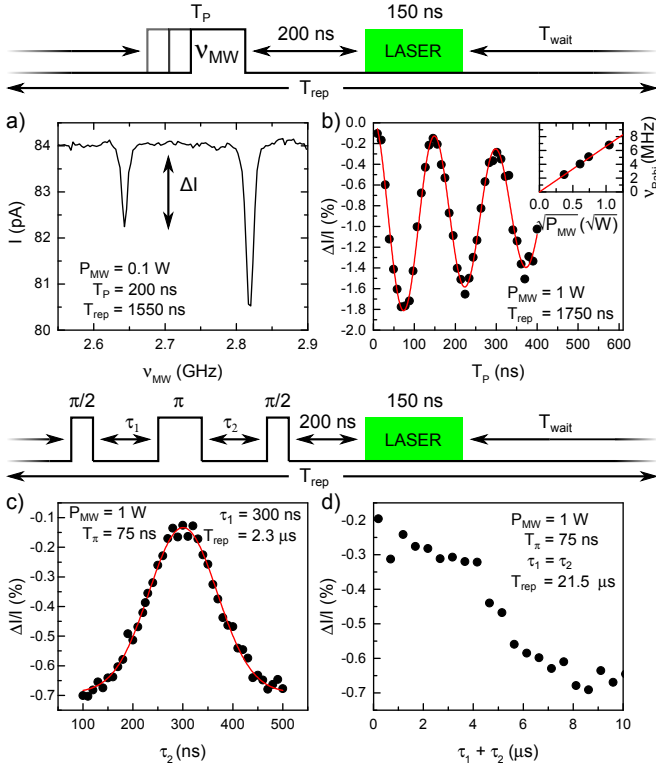


Figure 2. a) Pulsed electrically detected magnetic resonance spectrum for $B_0 \parallel \langle 111 \rangle$. b) Rabi oscillations in the contrast $\Delta I/I$ (symbols) with fit of an exponentially decaying cosine (line). The inset shows the frequency of Rabi oscillations (symbols) measured at different microwave powers and a linear fit (line). c) Spin echo measurement (symbols) with fit of a Gaussian (line). d) Echo decay measurement showing the first ESEEM decay. The pulse sequences used for the measurements are shown on top of the respective figure. T_π is the length of a π pulse.

(AOM) and observe the resulting photocurrent between two interdigit Schottky contacts, biased with a voltage of 5 V. The contacts (finger width 5 μm , finger-to-finger distance 10 μm) consist of a 10-nm-thick titanium layer and a 80-nm-thick gold layer, deposited on the diamond surface after cleaning it in a $\text{H}_2\text{SO}_4/\text{H}_2\text{O}_2$ mixture, followed by an oxygen plasma treatment. The photocurrent through the sample is measured using a transimpedance amplifier (amplification 1 G V A^{-1} , bandwidth 10 Hz). Depending on the measurement we use a 5x, a 10x or a 100x objective, with numeric apertures of 0.15, 0.30 and 0.80 and diffraction limited spot sizes of 3500 nm, 1800 nm and 670 nm, resp. The microwave with frequency ν_{MW} for spin manipulation is delivered to the sample using a wire next to the interdigit contact structure (cf. Fig. 1 b)).

We first demonstrate that coherent control of the NV^- centers can be detected electrically using the pulse sequence shown on top of Fig. 2 a) and b). To excite electron spin resonance (ESR) transitions, the se-

quence starts with a microwave pulse with power P_{MW} and varying duration T_p . This initializes the spin of the NV^- $^3\text{A}_2$ ground state. After a brief delay an optical excitation pulse follows (10x objective, light power of 210 mW during the optical pulse). Furthermore, an external magnetic field of $B_0 = 8.1 \text{ mT}$ is applied to the sample parallel to one of the $\{111\}$ axes via a permanent magnet so that only one crystallographic NV^- direction can be addressed. Figure 2 a) shows the pulsed electrically detected magnetic resonance (pEDMR) spectrum obtained under these conditions, monitoring the dc current through the interdigit contact structure. In contrast to previous pEDMR experiments on silicon and organic semiconductors, where the spin dependence of comparatively slow recombination or hopping processes is monitored via a boxcar integration of the current transients following the spin manipulation [15–19], the much faster photoionization and spin state initialization allows this vastly simpler direct detection of the spin signal in the dc current. As an example, the pulse repetition time T_{rep} is 1.5 μs in Fig. 2 a). On a background photocurrent level of $I = 84 \text{ pA}$ resonant decreases of the photocurrent are observed at $\nu_{\text{MW}} = 2.643 \text{ GHz}$ and 2.818 GHz , corresponding to one $\{111\}$ orientation parallel to the B_0 field and three off-axis $\{111\}$ orientations, resp. The resonant change of the current of $\Delta I = -1.5 \text{ pA}$ at 2.643 GHz corresponds to a relative spin-dependent current change (contrast) of $\Delta I/I = -1.8 \%$.

Rabi oscillations are observed when the length T_p of the microwave pulse is changed, adjusting the waiting time T_{wait} to keep T_{rep} constant at 1750 ns. Figure 2 b) shows the expected oscillatory dependence of $\Delta I/I$ on T_p . That indeed Rabi oscillations are obtained is demonstrated in the inset of Fig. 2 b), where the characteristic linear dependence of the oscillation frequency ν_{Rabi} on $\sqrt{P_{\text{MW}}}$ and, therefore, on the microwave magnetic field B_1 is observed. The Rabi oscillations exhibit an effective dephasing time of 600 ns, in accordance with other results on diamond with neutral isotope composition [20, 21]. In all experiments represented in Fig. 2 b) to d) $\Delta I/I$ was determined by cycling the microwave frequency between the resonant $\nu_{\text{MW}} = 2.643 \text{ GHz}$ and two nonresonant frequencies 2.61 GHz and 2.68 GHz, resulting in a low-frequency lock-in amplification [22].

The pulsed electrical detection scheme developed here also allows to detect spin echos, e.g., by using the pulse sequence depicted on top of Fig. 2 c) and d). As in the case of optically detected magnetic resonance (ODMR) [23, 24] and other pEDMR [25] experiments, the corresponding Hahn echo sequence needs to be extended by a final $\pi/2$ pulse, which projects the coherence echo to a polarisation accessible to optical or electrical readout. Figure 2 c) shows the echo in the contrast $\Delta I/I$ as a function of τ_2 for a fixed $\tau_1 = 300 \text{ ns}$. At $\tau_1 = \tau_2$ the total microwave pulse applied equals a nutation of 2π , so

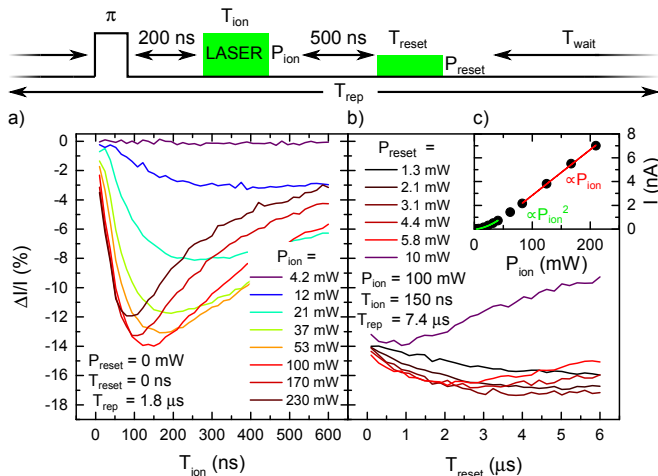


Figure 3. a) Contrast $\Delta I/I$ for a π microwave pulse as a function of the pulse length T_{ion} of the ionization pulse for different ionization pulse powers P_{ion} . b) $\Delta I/I$ as a function of the pulse length T_{reset} of an additional reset pulse for different reset pulse powers P_{reset} . The pulse sequence used is shown on top of the figure. c) Photocurrent through the sample as a function of the laser power. The green line is a fit of a polynomial of degree two, the red line is a fit of a linear function.

that the contrast is minimal, in full agreement with Fig. 2 b). For τ_2 significantly smaller or longer than τ_1 , no coherence echo is formed and the final $\pi/2$ projection pulse leads to an equal distribution of spin states which favor or which do not favor photoionization [25, 26]. Indeed, a maximum $\Delta I/I$ of -0.7% is observed for $\tau_1 \ll \tau_2$ or $\tau_1 \gg \tau_2$, in reasonable agreement with the contrast for $\pi/2$ pulses found in the Rabi oscillation experiment.

Finally, these echo experiments can also be performed as a function of total evolution time $\tau_1 + \tau_2$ with $\tau_1 = \tau_2$, giving access, e.g., to decoherence and to weak hyperfine interaction via electron spin echo envelope modulation (ESEEM). Figure 2 d) shows such an echo decay experiment on the 2.643 GHz resonance where the decay is caused by ESEEM [27]. Again, the pulse sequence repetition time is kept constant, the long times $\tau_1 + \tau_2$ necessary for this experiment reduce the signal-to-noise ratio. Nevertheless, the experiments summarized in Fig. 2 clearly demonstrate that all fundamental coherent experiments can be performed on the NV^- center with the electrical readout scheme developed here.

We now turn to study the readout contrast that can be obtained by pulsed electric readout. We therefore place ourselves at $B_0 = 0$, where all four NV^- orientations merge into a single resonance at $\nu_{\text{MW}} = 2.87$ GHz, and where we can essentially flip NV^- with all orientations into state $|2\rangle$ by a microwave π pulse of 75 ns length using $P_{\text{MW}} = 1$ W. Under these conditions we study the readout contrast as a function of both the duration T_{ion} and intensity P_{ion} of the readout light pulse (Fig. 3

top), keeping illumination as homogeneous as possible by widening the laser beam with the 5x objective to a spot size of 3800 nm.

Figure 3 a) plots $\Delta I/I$ versus T_{ion} for different P_{ion} . For each power we find an optimum pulse length between a regime of too short pulses, where the ionization of NV^- mostly takes place on a timescale faster than the shelving process suppressing the spin selection via the ISC, and too long pulses, where mostly NV^- contribute to the current which have lost their spin information by a decay through the ISC or by a preceding ionization. Optimizing P_{ion} and T_{ion} for the sample studied, we reach an optimum contrast of -14% at an intermediate power of 100 mW. As will be discussed below, this value is probably limited by ionization of background substitutional nitrogen donors (N_s^0) [13, 28].

The pulse powers and lengths optimal for readout may not be optimal for initialization and conversion of NV^0 to NV^- . Therefore in Fig. 3 b) we introduce a second laser pulse to separate the ionization process from the NV^- initialization. Here $\Delta I/I$ is plotted against the reset pulse length T_{reset} for different reset pulse powers P_{reset} . Small reset pulse powers improve $\Delta I/I$ for increasing T_{reset} . The optimal $P_{\text{reset}} = 3.1$ mW leads to a maximal $\Delta I/I$ of -17% which is reached for T_{reset} longer than $3 \mu\text{s}$. For higher P_{reset} the reset pulse itself starts to ionize the NV^- centers which leads to a decrease of $\Delta I/I$ since the NV^- have already undergone spin-dependent ionization or a decay through the ISC which eradicates all spin information.

We can quantitatively reproduce these observations by a Monte-Carlo model of the NV^- center's optical cycle together with photoionization and recharging of the NV^0 (Fig. 1 c)) using the partial lifetimes of Ref. 29. The excitation time t_{ex} from the $^3\text{A}_2$ ground state of the NV^- to its ^3E excited state, the characteristic time $a \cdot t_{\text{ex}}$ of the ionization process and the lifetime of the ionized state t_{NV^0} are used as parameters in the simulation. The simulation is repeated 1 million times for each starting state. Whenever the simulation transitions from NV^- to NV^0 or from NV^0 to NV^- , the generation of an electron or a hole in the respective bands at that time is recorded. Following the treatment in Ref. 30 the photocurrent through the diamond sample is $I = eG\frac{\tau}{T_r}$, with the elemental charge e , the charge carrier generation rate G , the typical charge carrier lifetime τ and the typical transit time T_r of the charge carriers through the photoconductor device. The ratio of τ and T_r is called the photoconductive gain $g = \frac{\tau}{T_r}$, so that $I = eGg$. Since the charge carrier generation rate is not constant throughout the measurement we replace G by its mean $\bar{G} = \frac{1}{T_{\text{ion}}} \int_0^{T_{\text{ion}}} G(t) dt = \frac{N}{T_{\text{ion}}}$ with N the number of charge carriers generated during the laser pulse time T_{ion} . To account for a background current I_{bg} , originating from the ionization of N_s^0 , we add the generation of electrons with a rate $G_{\text{N}_s^0} = a_{\text{bg}}/t_{\text{ex}}$ which allows to parametrize

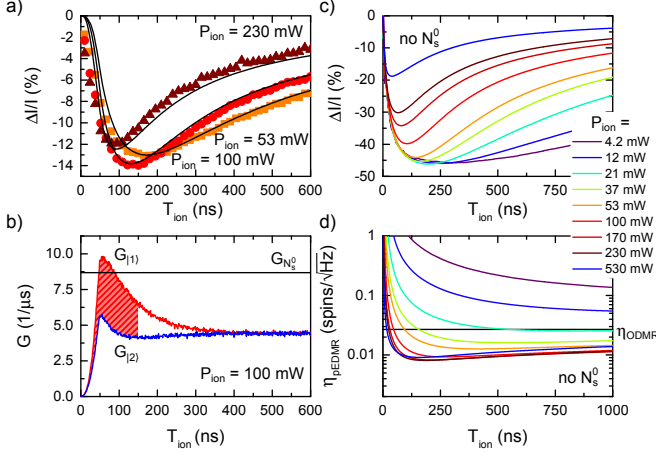


Figure 4. a) Contrast $\Delta I/I$ as a function of the length of the ionization pulse T_{ion} for three pulse powers taken from Fig. 3 and simultaneous fit of a Monte-Carlo simulation (black lines). b) Simulated charge carrier generation rate $G_{|1\rangle}$ and $G_{|2\rangle}$ plotted as a function of the time during the ionization pulse T_{ion} for starting states $|1\rangle$ and $|2\rangle$, resp. The black line depicts a constant background charge carrier generation rate $G_{N_s^0}$ originating from substitutional nitrogen donors. c) Simulated $\Delta I/I$ as function of T_{ion} for different P_{ion} under optimal conditions. d) Sensitivity η_{pEDMR} as a function of T_{ion} for different P_{ion} under optimal conditions. η_{ODMR} marks the typical ODMR sensitivity.

its dependence on the optical power. Microwave pulse imperfections yielding a mixture between $|1\rangle$ and $|2\rangle$ at the start of the experiment are described by a parameter p multiplied with the contrast curve. The contrast then becomes

$$\frac{\Delta I}{I} = p \frac{I_{|2\rangle} - I_{|1\rangle}}{I_{|1\rangle} + I_{\text{bg}}} = p \frac{\bar{G}_{|2\rangle} - \bar{G}_{|1\rangle}}{\bar{G}_{|1\rangle} + G_{N_s^0}} = p \frac{N_{|2\rangle} - N_{|1\rangle}}{N_{|1\rangle} + \frac{a_{\text{bg}}}{t_{\text{ex}}} T_{\text{ion}}}, \quad (1)$$

where the subscript $|1\rangle$ or $|2\rangle$ denotes the respective value for the initial states $|1\rangle$ and $|2\rangle$.

This term is fitted simultaneously to the data presented in Fig. 3 for the three laser powers of 53 mW, 100 mW and 230 mW using the Nelder-Mead simplex algorithm. The fit parameters a , a_{bg} , p and t_{NV^0} are used globally for all fits while $t_{\text{ex}} = t_{\text{ex,fit}} \cdot 100 \text{ mW} / P_{\text{ion}}$ is scaled according to the laser power P_{ion} used in the different experiments. To keep the complexity of the simulation down we use only one t_{NV^0} for all three fits which overestimates the generated photocurrent for small laser powers and vice versa. Figure 4 a) compares $\Delta I/I$ and the fit of the Monte-Carlo simulation, which are in very good agreement. We find $t_{\text{ex,fit}} = 22 \text{ ns}$, $a = 1.1$, $a_{\text{bg}} = 0.19$, $p = 0.75$ and $t_{\text{NV}^0} = 10 \text{ ns}$. A t_{ex} in the range of tens of ns is in agreement with the onset of a saturation in the photocurrent at $P_{\text{ion}} = 100 \text{ mW}$ (cf. Fig. 3 c)) which we expect to happen at the point where the excitation time from $|1, 2\rangle$ to $|3, 4\rangle$ reaches the partial

lifetime for the states $|3, 4\rangle$ to the state $|1, 2\rangle$. $p < 1$ is probably caused by the limited pulse fidelity at $B_0 = 0$, since differently oriented NV^- centers have different Rabi frequencies.

The model and the parameters determined allow us to simulate the charge carrier generation dynamics in our sample during a laser pulse. Figure 4 b) shows the charge carrier generation rate $G_{|1\rangle}(t)$ and $G_{|2\rangle}(t)$ for $P_{\text{ion}} = 100 \text{ mW}$. The horizontal line depicts a background current originating from N_s^0 at $G_{N_s^0} = 8.6 \mu\text{s}^{-1}$. For times bigger than 400 ns all spin-dependent signal is lost and the system is in a steady state with $\tilde{G}_{|1\rangle} = \tilde{G}_{|2\rangle} = 4.5 \mu\text{s}^{-1}$, each at about 1/2 the charge carrier generation rate originating from N_s^0 . For pulsed illumination with a pulse length $T_{\text{ion}} = 150 \text{ ns}$ we find $N_{|1\rangle} = 1.0$, $N_{|2\rangle} = 0.6$ and an N_s^0 background of 1.3 by integration over the curves. Therefore, even at high laser powers, the contrast is limited by N_s^0 ionization.

In order to find the limits of our detection method in samples free of N_s^0 background we simulate $\Delta I/I$ without a background photocurrent, with instantaneous AOM turn-on, and with $p = 1$. Figure 4 c) plots the contrast $\Delta I/I$ simulated under these conditions versus T_{ion} . Again, the $\Delta I/I$ has an optimal T_{ion} for each P_{ion} . The most notable difference is the maximal contrast of $\Delta I/I = -46\%$ which is predicted for a laser power of 21 mW.

However, we expect maximum sensitivity to be obtained for rather different optical pulse conditions. A sensitivity η is usually defined by $\eta = \frac{1}{\text{SNR}} \cdot \frac{N}{\sqrt{\Delta f}}$, with SNR the signal-to-noise ratio, N the number of spins and Δf the detection bandwidth of the particular experiment [31]. For ODMR we find the SNR using Poissonian statistics where the difference in photoluminescence (PL) counts $\Delta cts = cts_{|1\rangle} - cts_{|2\rangle}$ for the different initial states is divided by the shot noise generated by the number of counts $\sqrt{cts_{|1\rangle}}$ of the bright initial state $|1\rangle$. For pEDMR we use the difference in the current ΔI divided by the sum of the shot noise generated by the total current $\sqrt{2eI\Delta f}$ [32] and the amplifier input noise $\delta I_{\text{amp}} \cdot \sqrt{\Delta f}$. With this we find

$$\eta_{\text{ODMR}} = \frac{\sqrt{N}}{c\sqrt{cts_{\text{single}}\Delta f}} \quad \text{and} \quad (2)$$

$$\eta_{\text{pEDMR}} = \frac{\sqrt{2eI_{\text{single}}N} + \delta I_{\text{amp}}}{cI_{\text{single}}}, \quad (3)$$

where the subscript single denotes the corresponding value for a single NV^- center and c is the contrast of the corresponding measurement. Figure 4 d) plots the simulated sensitivity η_{pEDMR} at a sequence repetition rate of 500 kHz and for a typical amplifier input noise of $0.2 \text{ fA}/\sqrt{\text{Hz}}$ versus T_{ion} . For each P_{ion} the sensitivity decreases (i.e. improves) with longer T_{ion} because of the increased current I_{single} and contrast c for longer

ionization pulse times. After reaching an optimal value η_{pEDMR} increases again since the decrease in contrast c cancels the effects of the higher currents. The expected optimal sensitivity of $0.008 \text{ spins}/\sqrt{\text{Hz}}$ for pEDMR is not reached for the laser power corresponding to the maximum contrast but rather for P_{ion} between 170 mW and 230 mW and $T_{\text{ion}} \approx 200 \text{ ns}$. For comparison, the sensitivity for a typical ODMR experiment on a single NV^- center with a countrate of 100 kcts/s, a contrast of 30 % and an integration time over the fluorescence of 300 ns is $\eta_{\text{ODMR}} = 0.027 \text{ spins}/\sqrt{\text{Hz}}$ which is marked by the black horizontal line in Fig. 4 d).

To put this sensitivity in absolute numbers: Using a 100x objective and 1.2 mW of laser power a cw photocurrent of 32 pA is generated in our sample. Comparing the PL observed on it and on a reference sample with single NV^- centers allows us to estimate the number of NV^- participating to about 130 so that each NV^- contributes a photocurrent of 240 fA. Simulations under the corresponding power of 30 mW for the 5x objective predict a current of 580 fA per NV^- , so that the photoconductive gain in our samples is $g = 0.35 < 1$ as expected for a metal-semiconductor-metal photodetector based on Schottky contacts. Under the optimized conditions given above (170 mW optical power for a 5x objective, 500 kHz repetition rate, $g = 0.35$, $T_{\text{ion}} = 200 \text{ ns}$, no background current, no pulse imperfections), a single NV^- should exhibit a $\Delta I = 54 \text{ fA}$ on a photocurrent of $I = 190 \text{ fA}$, which should be easily measurable. This corresponds to a 'count rate' of 1.2 Mcts/s elementary charges at a spin contrast of 30 %, numbers which are not reached for photons in conventional detection setups

In summary, using a combination of pulsed photoionization and pulsed spin manipulation, we have demonstrated electrical readout of the coherent control of an ensemble of NV^- centers. With the help of a Monte-Carlo simulation we have improved our understanding of the photoionization dynamics and find that single-spin (multi-shot) detection should be feasible electrically, possibly with a higher sensitivity than optically. These results motivate a range of further studies, in particular into the relative benefits of photoconductors with ohmic or Schottky contacts and into more advanced photoionization schemes using lasers with different photon energies [28, 33, 34], which could lead to higher ionization efficiencies and a better understanding of the dynamics. Furthermore, EDMR based on photoionization should be transferable to other defects and other host materials such as SiC, which might allow even easier integration of electrical spin readout, e.g., with bipolar device structures.

This work was supported financially by Deutsche Forschungsgemeinschaft via FOR 1493 (STU139/11-2), SPP 1601 (BR 1585/8-2) and Emmy Noether grant RE 3606/1-1.

* florian.hrubesch@wsi.tum.de

† friedemann.reinhard@wsi.tum.de

‡ brandt@wsi.tum.de

- [1] N. Bar-Gill, L. M. Pham, A. Jarmola, D. Budker, and R. L. Walsworth, *Nature Communications* **4**, 1743 (2013).
- [2] A. Gruber, A. Dräbenstedt, C. Tietz, L. Fleury, J. Wrachtrup, and C. v. Borczyskowski, *Science* **276**, 2012 (1997).
- [3] J. M. Taylor, P. Cappellaro, L. Childress, L. Jiang, D. Budker, P. R. Hemmer, A. Yacoby, R. Walsworth, and M. D. Lukin, *Nature Physics* **4**, 810 (2008).
- [4] T. Wolf, P. Neumann, K. Nakamura, H. Sumiya, T. Ohshima, J. Isoya, and J. Wrachtrup, *Physical Review X* **5**, 041001 (2015).
- [5] V. M. Acosta, E. Bauch, M. P. Ledbetter, A. Waxman, L.-S. Bouchard, and D. Budker, *Physical Review Letters* **104**, 070801 (2010).
- [6] P. Maletinsky, S. S. Hong, M. Grinolds, B. Hausmann, M. D. Lukin, R. L. Walsworth, M. Loncar, and A. Yacoby, *Nature Nanotechnology* **7**, 320 (2012).
- [7] F. Shi, Q. Zhang, P. Wang, H. Sun, J. Wang, X. Rong, M. Chen, C. Ju, F. Reinhard, H. Chen, J. Wrachtrup, J. Wang, and J. Du, *Science* **347**, 1135 (2015).
- [8] V. R. Manfrinato, L. Zhang, D. Su, H. Duan, R. G. Hobbs, E. A. Stach, and K. K. Berggren, *Nano Letters* **13**, 1555 (2013).
- [9] N. R. Jungwirth, Y. Y. Pai, H. S. Chang, E. R. MacQuarrie, K. X. Nguyen, and G. D. Fuchs, *Journal of Applied Physics* **116**, 043509 (2014).
- [10] D. J. Christle, A. L. Falk, P. Andrich, P. V. Klimov, J. U. Hassan, N. T. Son, E. Janzén, T. Ohshima, and D. D. Awschalom, *Nature Materials* **14**, 160 (2015).
- [11] M. Widmann, S.-Y. Lee, T. Rendler, N. T. Son, H. Fedder, S. Paik, L.-P. Yang, N. Zhao, S. Yang, I. Booker, A. Denisenko, M. Jamali, S. A. Momenzadeh, I. Gerhardt, T. Ohshima, A. Gali, E. Janzén, and J. Wrachtrup, *Nature Materials* **14**, 164 (2015).
- [12] A. Brenneis, L. Gaudreau, M. Seifert, H. Karl, M. S. Brandt, H. Huebl, J. A. Garrido, F. H. L. Koppens, and A. W. Holleitner, *Nature Nanotechnology* **10**, 135 (2015).
- [13] E. Bourgeois, A. Jarmola, P. Siyushev, M. Gulka, J. Hruby, F. Jelezko, D. Budker, and M. Nesladek, *Nature Communications* **6**, 8577 (2015).
- [14] P. Siyushev, H. Pinto, M. Vörös, A. Gali, F. Jelezko, and J. Wrachtrup, *Physical Review Letters* **110**, 167402 (2013).
- [15] C. Boehme and K. Lips, *Physical Review B* **68**, 245105 (2003).
- [16] A. R. Stegner, C. Boehme, H. Huebl, M. Stutzmann, K. Lips, and M. S. Brandt, *Nature Physics* **2**, 835 (2006).
- [17] W. Harnett, C. Boehme, S. Schaefer, K. Huebener, K. Fostiropoulos, and K. Lips, *Physical Review Letters* **98**, 216601 (2007).
- [18] F. Hoehne, L. Dreher, M. Suckert, D. P. Franke, M. Stutzmann, and M. S. Brandt, *Physical Review B* **88**, 155301 (2013).
- [19] A. J. Kupijai, K. M. Behringer, F. G. Schaeble, N. E. Galfe, M. Corazza, S. A. Gevorgyan, F. C. Krebs, M. Stutzmann, and M. S. Brandt, *Physical Review B* **92**, 245203 (2015).

- [20] A. J. Parker, H.-J. Wang, Y. Li, A. Pines, and J. P. King, arXiv:1506.05484 (2015).
- [21] N. Mizuochi, P. Neumann, F. Rempp, J. Beck, V. Jacques, P. Siyushev, K. Nakamura, D. J. Twitchen, H. Watanabe, S. Yamasaki, F. Jelezko, and J. Wrachtrup, *Physical Review B* **80**, 041201 (2009).
- [22] F. Hoehne, L. Dreher, J. Behrends, M. Fehr, H. Huebl, K. Lips, A. Schnegg, M. Suckert, M. Stutzmann, and M. S. Brandt, *Review of Scientific Instruments* **83**, 043907 (2012).
- [23] W. G. Breiland, C. B. Harris, and A. Pines, *Physical Review Letters* **30**, 158 (1973).
- [24] L. Childress, M. V. G. Dutt, J. M. Taylor, A. S. Zibrov, F. Jelezko, J. Wrachtrup, P. R. Hemmer, and M. D. Lukin, *Science* **314**, 281 (2006).
- [25] H. Huebl, F. Hoehne, B. Grolik, A. R. Stegner, M. Stutzmann, and M. S. Brandt, *Physical Review Letters* **100**, 177602 (2008).
- [26] D. P. Franke, F. Hoehne, L. S. Vlasenko, K. M. Itoh, and M. S. Brandt, *Physical Review B* **89**, 195207 (2014).
- [27] P. L. Stanwix, L. M. Pham, J. R. Maze, D. Le Sage, T. K. Yeung, P. Cappellaro, P. R. Hemmer, A. Yacoby, M. D. Lukin, and R. L. Walsworth, *Physical Review B* **82**, 201201 (2010).
- [28] E. Bourgeois, E. Londero, K. Buczak, Y. Balasubramanian, G. Wachter, J. Stursa, K. Dobes, F. Aumayr, M. Trupke, A. Gali, and M. Nesladek, arXiv:1607.00961 (2016).
- [29] L. Robledo, H. Bernien, T. v. d. Sar, and R. Hanson, *New Journal of Physics* **13**, 025013 (2011).
- [30] A. Rose, *Concepts in Photoconductivity and Allied Problems* (Interscience Publishers, New York, 1963).
- [31] G. Boero, M. Bouterfas, C. Massin, F. Vincent, P.-A. Besse, R. S. Popovic, and A. Schweiger, *Review of Scientific Instruments* **74**, 4794 (2003).
- [32] R. Müller, *Rauschen* (Springer Verlag, Berlin, 1990).
- [33] B. Shields, Q. Unterreithmeier, N. de Leon, H. Park, and M. Lukin, *Physical Review Letters* **114**, 136402 (2015).
- [34] D. A. Hopper, R. R. Grote, A. L. Exarhos, and L. C. Bassett, arXiv:1606.06600 (2016).